1.0

4.5

2.8   2.5

3.2   2.2

3.6

4.0   2.0

1.1

1.8

1.25   1.4   1.6

MICROCOPY RESOLUTION TEST CHART

Office of Naval Research

Contract N00014-76-C-0060 NR 064-478

Technical Report No. 41

DYNAMIC CRACK CURVING - A PHOTOELASTIC EVALUATION

by

M. Ramulu and A. S. Kobayashi

October 1981

Department of Mechanical Engineering

College of Engineering

University of Washington

81 11 12 058

DYNAMIC CRACK CURVING - A PHOTOELASTIC EVALUATION

by

M. Ramulu* and A. S. Kobayashi**

. A dynamic crack curving criterion, which is valid under combined modes
I and II or mode I loading and which is based on either the maximum circum-
ferential stress or minimum strain energy density factor at a reference
distance of $r_0 = \frac{1}{128\pi}(\frac{K_1}{\sigma_{ox}})^2 v^2$ (c, c_1, c_2) crack deformation, is developed.
Directional stability of a mode I crack propagation is attained when
$r_0 > r_c$, where r_c for Homalite-100 was determined from dynamic photoelastic
experiments. In the presence of mode II crack deformation, positive remote
stress component, i.e., $\sigma_{ox} > 0$ and negative remote stress component, i.e.,
$\sigma_{ox} < 0$, was found to enhance and supress crack curving, respectively.

*Graduate student, University of Washington, Department of Mechanical
Engineering, Seattle, WA 98195

**Professor, University of Washington, Department of Mechanical Engineer-
ing,Seattle, WA 98195

INTRODUCTION:

Crack extension and fracture criteria under combined tension and shear loading are based on either energy or maximum circumferential stress criteria. The maximum circumferential stress, $\sigma_{\theta\theta}$, criterion was first used by Erdogan and Sih [1], for predicting the direction, θ_c, of an angled crack. Williams and Ewing [2] extended this theory by incorporating the second order term of σ_{ox} in the Williams eigenfunction expansion. Finnie and Saith [3] corrected an oversight in the above angle crack analysis and obtained an improved agreement between predicted and experimental data. Streit and Finnie [4] further proposed a crack stability model where directional stability of a mode I crack propagation is maintained when a characteristic distance of r_0 from the crack tip satisfies $r_0 \geq r_c$, where r_c is a critical distance ahead of the crack tip. Cotterell and Rice [5] derived the necessary condition for a slightly curved, quasi-static, mixed mode crack growth where stability of crack growth was also governed by σ_{ox}. Karihaloo et al. [6], recently showed that crack curving can occur without kinking under vanishing σ_{ox} and mode II stress intensity factor, but with non-vanishing derivative of K_{II} with respect to the crack length.

As for the energy approach, Hussain et al., [7], Palaniswamy and Knauss [8], Gupta [9], Wu [10], and Nemat-Nasser et al. [11-12], among others, predicted the direction of a kinked crack based on a maximum strain energy release rate criterion. Sih [13], on the other hand, proposed the S-theory where the direction of crack kinking coincides with the direction of the minimum strain energy density. Theocaris and Andrianopoulos [14], recently modified the S-theory by designating its mean value, $\bar{S}$, the critical quantity for crack initiation, under mixed mode crack tip deformation.

The above papers all relate to quasi-static crack extension. As for dynamic crack curving criterion, Yoffe [15] and Sih [16], used the maximum dynamic circumferential stress theory and minimum strain energy density theory, respectively to explain crack branching phenomena.

The objective of the present study is to derive a dynamic crack curving criterion applicable to both mode I and combined modes I and II crack tip deformation. To this goal, dynamic extension of two static crack curving criteria, that is the maximum circumferential stress criterion and the minimum strain energy density criterion at a critical distance r_c, was considered. The developed theoretical relations were evaluated numerically and the influence of σ_{ox} and crack velocity on crack curving direction were deduced. Crack curving angles predicted by the two dynamic crack curving criteria were then compared with experimental results, obtained from past dynamic photoelastic investigation.

DYNAMIC CRACK CURVING CRITERIA

Elasto-dynamic Crack Tip Stress Field

The dynamic crack curving criteria, are derived from the near field, mixed mode elasto-dynamic state of stress associated with a crack tip propogating at constant velocity. This dynamic state of stress is given by Freund (17,18) in terms of local rectangular and polar co-ordinates of (x,y) and (r,θ), respectively, with origin at the crack tip, and the mode I and II dynamic stress intensity factors, K_I and K_{II}*, respectively. The authors [19] have added to Freund's near field, dynamic state of stress the second order term of σ_{ox} which is acting parallel to the direction of crack extension. This dynamic singular crack tip stress field under mixed mode loading for small θ values differs from the corresponding static stress field in that the largest principal singular tensile stress acts parallel to the x-axis, a fact which not only contributes to crack curving but also to dynamic crack branching. Furthermore, this region

---

*The superscript "dyn" to identify dynamic stress intensity factor will not be used in this paper, since all quantities refer to dynamic values.

ahead of the running crack where $|\sigma_{xx}| > \sigma_{yy}$ increases with increases in crack speed and σ_{ox} even under pure mode-II crack tip deformation [19]. This inevitable involvement of σ_{ox} forms the basis of incorporating σ_{ox} in the dynamic crack curving criteria presented in this paper.

Maximum Circumferential Stress Theory

The angle, θ_c, at which circumferential stress, $\sigma_{\theta\theta}$, is maximum, can be obtained from the following,

$$\frac{\partial \sigma_{\theta\theta}}{\partial \theta} = 0 \qquad \sigma_{\theta\theta} > 0 \tag{1}$$

where the added $\sigma_{\theta\theta} > 0$ is to assure fracture under tensile state of stress. Equation (1), when evaluated in conjunction with a pure mode I dynamic crack tip state of stress will yield a transcendental relation between the critical values of θ and r. Furthermore, by setting $\theta = 0$ in Equation (1), we obtain

$$r_0 = \frac{1}{128\pi} \left\{ \left(\frac{K_I}{\sigma_{ox}}\right) V(c, c_1, c_2) \right\}^2 \tag{2a}$$

where $V(c, c_1, c_2) = \left[B_I(c) \left\{ -(1+S_2^2)(2-3S_1^2) - \frac{4S_1 S_2}{1+S_2^2}(14+3S_2^2) - 16S_1(S_1 - S_2) \right. \right.$ $\tag{2b}$

$$\left. \left. +16(1+S_2^2) \right\} \right]$$

$$B_I(c) = \left\{ \frac{(1+S_2^2)}{4S_1 S_2 - (1+S_2^2)^2} \right\} \tag{2c}$$

$$S_1^2 = \left[1 - \frac{c^2}{c_1^2} \right] \quad ; \quad S_2^2 = \left[1 - \frac{c^2}{c_2^2} \right] \tag{2d}$$

and c, c_1 and c_2 are the crack velocity, dilatational wave velocity, and distortional wave velocity, respectively. It can be easily shown that for zero crack velocity or c = o, Equation (2a) reduces to Streit and Finnie's solution [14] of $r_0 = \frac{9}{128\pi} \left(\frac{K_I}{\sigma_{ox}}\right)^2$

Figure 1 shows the velocity effect on r_0 which is plotted in a non-dimensional form of $\left[\sqrt{r_0}\ \frac{\sigma_{ox}}{K_I}\right]$ where the dynamic r_0 is always less than the corresponding static r_0 at experimentally observed crack velocities of $0 < c \leq 0.33$ and is insensitive to the sign of σ_{ox}. The terminal crack velocity of $c/c_1 \doteq 0.325$, in Figure 1 where $r_0 = 0$ concides with the terminal velocity predicted by Yoffe [15].

Minimum Strain Energy Density Theory

According to this theory, the crack will extend to the location of the minimum strain energy density factor, S_{min}, or

$$\frac{\partial S}{\partial \theta} = 0 \text{ at } \theta = \theta_c \tag{3}$$

The intensity of the strain energy density, S, for the state of plane strain can be written as

$$S = r_0 \frac{(1+\nu)}{2E}\left[(1-\nu)(\sigma_{xx}^2 + \sigma_{yy}^2) - 2\nu(\sigma_{xx} \cdot \sigma_{yy}) + 2\sigma_{xy}^2\right] \tag{4}$$

where E and ν are the modulus of elasticity and Poisson's ratio, respectively. Substituting the dynamic mixed mode crack tip stresses into Equation (4) and then into Equation (3) yields

$$\left\{\left[(1-\nu)\sigma_{xx} - \nu\sigma_{yy}\right]\frac{\partial \sigma_{xx}}{\partial \theta} + \left[(1-\nu)\sigma_{yy} - \nu\sigma_{xx}\right]\frac{\partial \sigma_{yy}}{\partial \theta} + 2\sigma_{xy}\frac{\partial \sigma_{xy}}{\partial \theta}\right\}$$

$$+ \sqrt{r_0}\ \sigma_{ox}\left\{(1-\nu)\frac{\partial \sigma_{xx}}{\partial \theta} - \nu\frac{\partial \sigma_{yy}}{\partial \theta}\right\} = 0 \tag{5}$$

By setting Poisson's ratio $\nu = 1/3$, $\sigma_{ox} = 0$ as a crack velocity of $c \rightarrow 0$ in Equations (5), the static angular predictions in Reference [13] are recovered. When a non-vanishing second order term of σ_{ox} is considered in Equation (5)

yields four θ_c values, a pair for S_{max} and another pair of S_{min} for given values of c, K_{II}/K_I, r_0 and σ_{ox}. Only the negative root of θ_c corresponding to positive K_{II}/K_I and the positive root of θ_c for negative K_{II}/K_I, to the tensile loading are of interest [13]. Numerical values of these θ_c will be discussed in the following section.

Actual evaluation of Equation (3) will show that curving of a straight crack propagating at the lower velocity can be considered only by incorporating the nonsingular term of σ_{ox} in the minimum strain energy density criteria. Such possibility of crack curving without K_{II} values and under the minimum strain energy criterion has not been considered by others.

Comparison of Maximum oo·and Minimum S Criterion

Figure 2 shows the predicted crack curving angles for crack velocities, c/c_1, from 0 to 0.25 by maximum stress and the minimum strain energy density criteria when σ_{ox} = 0. Without the second order term, both criteria predicted the same crack curving angles for much of the crack velocity range. Although the crack curving angle at higher crack velocities are significant for lower crack velocities of $c/c_1 \leq 0.15$, the predicted crack curving angle, which is referred to as fracture angle from hereon, is almost constant and is in close agreement with corresponding static fracture angles.

The effects of the non-singular term of σ_{ox} and reference radius r_0 in predicting the fracture angle by both maximum $\sigma_{\theta\theta}$ and minimum S theories at various crack velocities are shown in Figure 3 for ν = 1/3, and K_{II}/K_I = -0.1, and σ_{ox}/K_I = -1.0 and 1.0. Note that fracture angle for negative σ_{ox}, are much smaller than those with positive σ_{ox}. Also, larger r_0 results in larger changes in the fracture angle. For larger values of r_0, the differences in predicted fracture angles due to maximum circumferential stress theory and minimum strain

energy density theory are larger at higher crack velocities. This importance of r_o value in characterizing the direction of the fracture angles is discussed in Reference [14].

EXPERIMENTAL VERIFICATION

Dynamic Isochromatics:

For a single, pure mode-I or combined modes I and II crack propagating at a constant velocity, the dynamic crack tip isochromatic patterns together with the predicted path are shown in Figure 4. Changes in the remote stress, σ_{ox}, results in backward or forward tilting of the dynamic isochromatics. For a given σ_{ox}, the change in the sign of K_{II}, results in a mirror image of the isochromatics. Detailed discussion of the changes in dynamic isochromatics with variations in K_{II}/K_I and σ_{ox}/K_I can be found in Reference [19].

Data Reduction Procedure

Experimentally determined dynamic isochromatics surrounding a running crack often exhibits moderate unsymmetry. Such photoelastic patterns were heretofore considered experimental abnormalities and were ignored by averaging the unsymmetric patterns during the data reduction process. Careful postmortem inspection of the fracture specimens, however, show that the higher magnitudes of σ_{ox} of isochromatics and slightly unsymmetric isochromatics are often associated with slightly curved crack patterns. With the development of a data reduction procedure [19] for evaluating dynamic K_{II} together with K_I and σ_{ox} values, it became possible to investigate the above criteria by extracting K_I and K_{II} and σ_{ox} from the previously recorded dynamic isochromatics surrounding running crack tips of curved cracks. An optimization method developed by the authors based on the overdeterministic least square procedure was also used to extract the dynamic three parameters K_I, K_{II} and σ_{ox} from the recorded dynamic photoelastic pattern surrounding a running crack [19,20].

The dynamic crack curving criteria developed for pure mode-I loading conditions require accurate determination of K_I and σ_{ox}. Accuracy of the data reduction procedure used in this investigation was verified by using the above data reduction procedure to calculate K_I and σ_{ox} from previously generated isochromatics generated by three parameters of K_I, σ_{ox}, and A_3 with $K_{II} = 0$ [21]. The recovered two dynamic parameters K_I and σ_{ox} agreed within $\pm$ 0.5% and $\pm$ 5%, respectively, with the given results. This series of numerical experiments showed that the two parameter characterization procedure involving K_I and σ_{ox} should describe reasonably well the stress field in the vicinity of a running crack tip.

The crack curving angle was measured along the crack path by averaging the measured crack curving angle on front and back surfaces of the fractured specimen since the crack surfaces of some of the curved cracks were not perpendicular to the specimen surfaces. The maximum variation between the front and back crack curving angles was about 3 degrees for severely curved cracks. Similar differences in out-of-phase crack curving were also observed by Williams et al., in their PMMA specimens [2].

Results

Figure 5 shows three frames out of a 16 frame dynamic photoelastic record of a curving crack in a Homalite-100 dynamic tear test (DTT) specimen of 9.58 mm (3/8 in) thick, 88.9 x 400 mm (3 1/2 x 15 in). This beam with a blunt initial crack of 6.4 mm (7/32 in) in length was impact loaded by a drop weight of 1.48 kg (3.25 lb) [22]. The crack emanated from the blunt saw-cut crack and propagated through much of the height of the beam prior to curving near the region of impact loading. Further details of the experimental setup, crack velocity measurements and dynamic calibration of the Homalite-100 material used are found in

Reference [22]. Figure 6 shows K_I, K_{II}, $\overline{\sigma_{ox}}$ and r_o which is computed by Equation (2), obtained from the dynamic photoelastic pattern preceding and immediately after the crack curving in Figure 5. K_{II} is negligible in comparison to K_I and at the point of instability and pronounced fluctuation in $\overline{\sigma_{ox}}$ is noted. After crack curving K_{II} and $\overline{\sigma_{ox}}$ increased while K_I and crack velocity dropped rapidly. r_o was close to 1.5 mm throughout crack propagation and reached a minimum value of $r_c \doteq 1$ mm during the onset of crack curving.

Figure 7 shows a slightly curved crack and the associated K_I, K_{II}, $\overline{\sigma_{ox}}$ and r_o in a fracturing 9.53 mm (3/8 in) thick, 254 x 254 mm (10 x 10 in) single-edge-notch (SEN) Homalite-100 specimen [23]. Gradual increase and decrease of K_I and a very small K_{II} with a rapid fluctuation of $\overline{\sigma_{ox}}$ and r_o are noted. Three SEN results were evaluated where K_I reached a maximum value, K_{II} was negligible and $\overline{\sigma_{ox}}$ was increasing prior to crack curving. At the onset of instability, a sudden drop in K_I and larger $\overline{\sigma_{ox}}$ with $K_{II} = 0$ are observed. r_o dropped sharply to an average value of 1.5 mm at the point of instability. This minimum r_o value will be referred to r_c which will be found to be a material parameter associated with dynamic crack curving. The small negative K_{II}, which appeared immediately after crack instability, resulted in a positive angle of crack curving. This result is not only in agreement with the analytically predicted angles in Figure 3 but is also in agreement with similar observation in crack curving under stable crack growth conditions [24]. The rapid oscillations of r_o in all the three SEN specimens appeared to be related to the rapid but opposing oscillations in $\overline{\sigma_{ox}}$.

Figure 8 shows a curved crack and the associated, K_I, K_{II}, $\overline{\sigma_{ox}}$ and r_o in a Homalite-100, wedge-loaded, rectangular double cantilever beam (WL-RDCB) specimen of 9.6 mm (3/8 in) thick and 76.2 x 152.4 mm (3 x 6 in) with a blunt initial crack of length 2.36 m (0.093 in). Experimental details of this series

of tests can be found in Reference [25]. Fluctuations in dynamic fracture para-meters K_I, K_{II}, $\overline{\sigma_{ox}}$ and r_o is noted all along the curved crack path. The crack curved continuously without any kinks and is a characteristic fracture path of DCB specimens.

Figure 9 shows five frames out of a 16-frame dynamic photoelastic record of a curving crack in a 9.53 mm (3/8 in) thick, 254 x 254 mm (10 x 10 in) Homa-lite-100 single edge notch (SEN) specimen loaded under fixed gripped tension. The crack emanated from a small precrack 150 μsec after impact by a flat-nosed projectile. The severe stress wave reflections in this specimen caused the crack to curve continuously in a zig-zag manner. Details of this experiment can be found in Reference [26]. Figure 10 shows the corresponding K_I, K_{II}, $\overline{\sigma_{ox}}$ and r_o variations associated with the unsymmetric dynamic isochromatics in this test. Severe stress wave loading caused the crack to curve immediately after propagation and r_c is about 1.35 mm at this crack kinking. Throughout crack propagation, $\overline{\sigma_{ox}}$ changed signs and is related to the zig-zagged crack path.

Fracture angles of curved cracks measured in nine dynamic photoelas' ,city tests and the corresponding fracture angles computed by the maximum $\sigma_{\theta\theta}$ and minimum S theories are summarized in the Table 1. Remarkable agreements in experimentally measured and numerically computed results by both the theories, using an experimentally measured $r_c \doteq 1.3$ mm for Homalite-100 are noted. Crack curving in our experiments for mode I, crack propagation ranged between $\pm 25^o$ to a minimum of 2° for severe to moderate curving.

DISCUSSIONS

The closed form elasticity solution for a circular arc crack under uniform stress field provides a siimple check on the accuracy of using the near field solution of a straight crack in the results cited above. The static solution given by Panasyuk and Brezhnitskiy [27] in the vicinity of a circular arc crack

with an included angle 2α differ with straight crack solution only by a multiplication factor of

$$K_I^{curved} = K_I^{straight} \cos\alpha/2 / (1+Sin^2\alpha/2) \qquad (6a)$$

$$K_{II}^{curved} = K_{II}^{straight} \sin\alpha/2 / (1+Sin^2\alpha/2) \qquad (6b)$$

$$\sigma_{ox}^{curved} = \sigma_{ox}^{straight} Sin^2\alpha/2 / (1+Sin\alpha/2) \qquad (6c).$$

where the superscripts "straight" and "curved" refer to crack tip parameters associated with a straight and curved crack, respectively. As an estimate of possible errors involved in using a straight crack solution to evaluate the fracture parameters of a curved crack were determined by least square fitting the above exact static solution of a curved crack and the corresponding solution for a straight crack to the two extreme curved cracks associated with the last data points in Figures 6 and 8. The resultant K_I, K_{II} and σ_{ox} of the straight crack solutions are within 10%, 28% and 6%, respectively of the corresponding solutions for circular arc cracks of $\alpha = 25$ and 28°. Thus, possible error introduced by using a second order dynamic crack tip state of stress of a straight crack in place of a curved crack should be negligible for most of the curved crack problems of $\alpha \doteq 5 \sim 10^o$ in this investigation.

The developed dynamic crack curving criterion shows the large σ_{ox} contributes to crack instability and is in agreement with Benbow and Roesler's conclusion involving static experiments [28]. Cotterell [29-31] referring to Williams analysis [32], showed that the crack path will be unstable when σ_{ox} is positive. The above static crack stability criterion [28-31] correlates well with the experimental results of DCB specimens but cannot explain dynamic crack curvings

in fracture specimens of SEN, CT, and DTT where σ_{ox} is negative. The proposed criterion for the directional stability of a propagating crack is independent of the sign of the σ_{ox}, and is thus applicable to all crack curving data considered in this paper.

As shown in Figure 3 the influence of non-singular stress is more pronounced for moderate values of r_o irrespective of the sign of K_{II}/K_I. This result re-emphasizes the importance of the non-singular stress term σ_{ox}, which, when neglected, can lead to inaccurate results as observed by Tirosh [33].

Considering the fact that dynamic photoelasticty experiments cited in this paper were conducted by four different investigators over a period of ten years with different shipments of Homalite-100, the consistent results of $r_c = 1.3$ mm is noticeable. In a critical review on r_c associated with the minimum S criterion of crack curving, Theocaris and Andriaopoulos (14) also determined experimentally $r_c = 1.3$ mm (0.05") for polymethylmethacrylate.

Finally, the crack curving criterion by Karihaloo et al. [12] requires that K_{II} be known immediately before and after crack curving. The lack of sensitivity in this analysis precluded precise variations of the very small K_{II} before or after crack curving and thus this crack curving could not be checked.

CONCLUSIONS

1. A dynamic crack curving criterion based on the directional stability of a running crack under pure mode-I loading is developed.

2. Dynamic fracture angle under pure mode I and mixed mode I and II conditions can be predicted by using either the maximum circumferential stress or the minimum strain energy density theories with the non-singular stress term σ_{ox}.

3. Positive σ_{ox} always enhances the crack curving and negative σ_{ox} reduces the fracture angle irrespective of the sign of K_{II}/K_I.

4. Experimental results with and without K_{II} proved that r_c is a material constant. The critical value of Homalite-100 is $r_c = 1.3$ mm (0.05 in).

ACKNOWLEDGEMENT

TABLE I
SUMMARY OF EXPERIMENTAL AND
THEORETICAL RESULTS

Total Number of Experiments:	9
Type of Fracture Specimen:	DTT, SEN, WL-RDCB
Number of Data Points:	81
Crack Velocity, c/c_1:	0.03 to 0.21
K_I (MPa m)	0.50 to 1.59
K_{II}/K_I	-0.22 to 0.18
$_{ox}/K_I$	-2.89 to 4.04
Experimental Fracture Angle Associated with Crack Curving	-20° to 26°
Theoretical Prediction of Fracture Angle	-20° to 25°
r_c (mm)	1.0 to 1.5

REFERENCES

1. Erdogan, F. and Sih, G. C., "On the crack extension in plates under plane loading and transverse shear", *Trans. ASME J. Basic Engrg 85*(D), 1963, pp. 519-527.

2. Williams, J. G. and Ewing, P. D., "Fracture under complex stress - The angled crack problem", *Int. J. Fracture Mech.8,* 1972, pp. 441-446.

3. Finnie, I. and Saith, A., "A note on the angled crack problem and the directional stability of crack", *Int. J. Fracture 9,* 1973, pp. 484-486.

4. Streit, R. and Finnie, I., "An Experimental Investigation of Crack-path Directional Stability", *Experimental Mechanics,* Vol. 20, No. 1, January 1980, pp. 17-23.

5. Cottrell, B. and Rice, J. R., "Slightly Curved or Kinked Cracks", *Int. J. Frac.* Vol. 11, No. 2, 1981, pp. 155-164.

6. Karihaloo, B. L., Keer, L. M., Nemat-Nasser, S. and Oranatnachai, A., "Approximate Description of Crack Kinking and Curving", ASME paper No. 81-APM-22.

7. Hussain, M. A., Pu, S. L., and Underwood, J., "Strain-Energy-Release Rate for a Crack Under Combined Mode I and Mode II", ASTM-STP-560, 1974, pp. 2-28.

8. Palaniswamy, K. and Knauss, W. G., "On the Problem of Crack Extension in Brittle Solids Under General Loading", *Mechanics Today 4,* edited by S. Nemat-Nasser, Pergamon Press, 1978, pp. 87-148.

9. Gupta, G. D., "Strain Energy Release Rate for Mixed Mode Crack Problem", ASME Paper No. 76-WA/PVP-7.

10. Wu, C. H., "Elasticity Problems of Slender Z-Crack", *Journal of Elasticity,* Vol. 8, 1978, pp. 183-205.

11. Hayashi, K. and Nemat-Nasser, S., "Energy Release Rate and Crack Kinking", *Int. J. of Solids and Structures,* Vol. 17, 1981, pp. 107-114.

12. Karihaloo, B. L., Keer, L. M. and Nemat-Nasser, S., "Crack Kinking Under non-Symmetric Loading", *Eng. Fract. Mechanics,* Vol. 13, 1980, pp. 879-888.

13. Sih, G. C., "A Special Theory of Crack Propagation", *Methods of Analysis and Solutions of Crack Problems,* Vol. 1, pp. 21-45, edited by G. C. Sih, Noordhoff International Publishing, Leyden, 1973.

14. Theocaris, P. S. and Andrianopoulos, N. P., "A Modified Strain Energy Density Criterion Applied to Crack Propagation", to be published in the ASME Journal of Applied Mechanics.

15. Yoffe, E. H., "The Moving Griffith Crack", Philosophical Magazine, Vol. 42, 1951, pp. 739-750.

16. Sih, G. C., "Dynamic Crack Problems: Strain Energy Density Fracture Theory", Elastodynamic Crack Problems, Vol. 4, pp. 17-37, ed. by G. C. Sih, Noordhoff International Publishing, Leyden, 1977.

17. Freund, L. B., "Dynamic Crack Propagation", The Mechanics of Fracture, Vol. 19, ed. by F. Erdogan, ASME, 1976, pp. 105-134.

18. Freund, L. B., "The Mechanics of Dynamic Shear Crack Propagation", Journal of Geophysical Research, Vol. 84, No. 35, 1978, pp. 2199-2209.

19. Kobayashi, A. S. and Ramulu, M., "Dynamic Stress Intensity Factors for Unsymmetric Dynamic Isochromatics", Experimental Mechanics", Vol. 21, Jan. 1981, pp. 41-48.

20. Kobayashi, A. S. and Ramulu, M., "Dynamic Mixed Mode Fracture", Proc. U.S.-Greece Symposium on Mixed Mode Fracture, ed. G. Sih and P. S. Theocaris, Noordhoff, Holland, 1981.

21. Kobayashi, A. S. and Mall, S., "Dynamic Fracture Toughness of Homalite-100", Experimental Mechanics, 18, 1, Jan. 1978, pp. 11-18.

22. Kobayashi, A. S. and Chan, C. F., "A Dynamic Photoelastic Analysis of Dynamic-tear-test Specimen", Experimental Mechanics, Vol. 16, No. 5, May 1976, pp. 176-181.

23. Bradley, W. B. and Kobayashi, A. S., "Fracture Mechanics - A Photo-elastic Investigation", Engineering Fracture Mechanics, Vol. 3, 1971, pp. 317-332.

24. Iida, S. and Kobayashi, A. S., "Crack Propagation Rate in 7075-T6 Plates Under Cyclic Tensile and Transverse Shear Loading", J. of Basic Engineering, Trans. of ASME, Vol. 91, Series D (4), Dec. 1964, pp. 764-769.

25. Kobayashi, A. S., Mall, S. and Lee, M. H., "Fracture Dynamics of Wedge-Loaded Double Cantilever Beam Specimen", Cracks and Fracture", ASTM STP, 601, June 1976, pp. 274-290.

26. Wade, B. G. and Kobayashi, A. S., "Photoelastic Investigation on the Crack Arrest Capability of Pretensioned Stiffened Panels", Exp. Mech-anics, 15, 1, 1975, pp. 1-9.

27. Panasyuk, V. V., Brezhnitskiy, L. T., _Voprosy Mechaniki_, Real nogo Tverdogo Tela No. 3, Naukova Dumka press, Kiev, 1965.

28. Benbow, J. J. and Roesler, F. C., "Experiments on Controlled Fractures", _Proc. Phys. Soc. 70_, Ser. B., 1957, pp. 201-211.

29. Cotterell, B., "Notes on the Paths and Stability of Cracks", _Int. J. Fracture Mech._, 2, 1966, pp. 526-533.

30. Cotterell, B., "On Fracture Path Stability in the Compact Tension Test", _Int. J. Fracture Mech._, 6, 1970, pp. 189-192.

31. Cotterell, B., "On Brittle Fracture Paths", _Int. J. Fracture Mech._, 1, 1965, pp. 96-103.

32. Williams, M. L. "On the Stress Distribution at the Base of a Stationary Crack", _J. of Applied Mech._, Vol. 24, 1957, pp. 109-116.

33. Tirosh, J., "Incipient Fracture Angle, Fracture Velocity and Critical Stress for Mixed Mode Loading", _Eng. Frac. Mech._, Vol. 9, 1977, pp. 607-616.

$$r_0 = \frac{1}{128\pi} \left(\frac{K_I}{\sigma_{ox}}\right)^2 \left[V(c, c_1, c_2)\right]^2$$
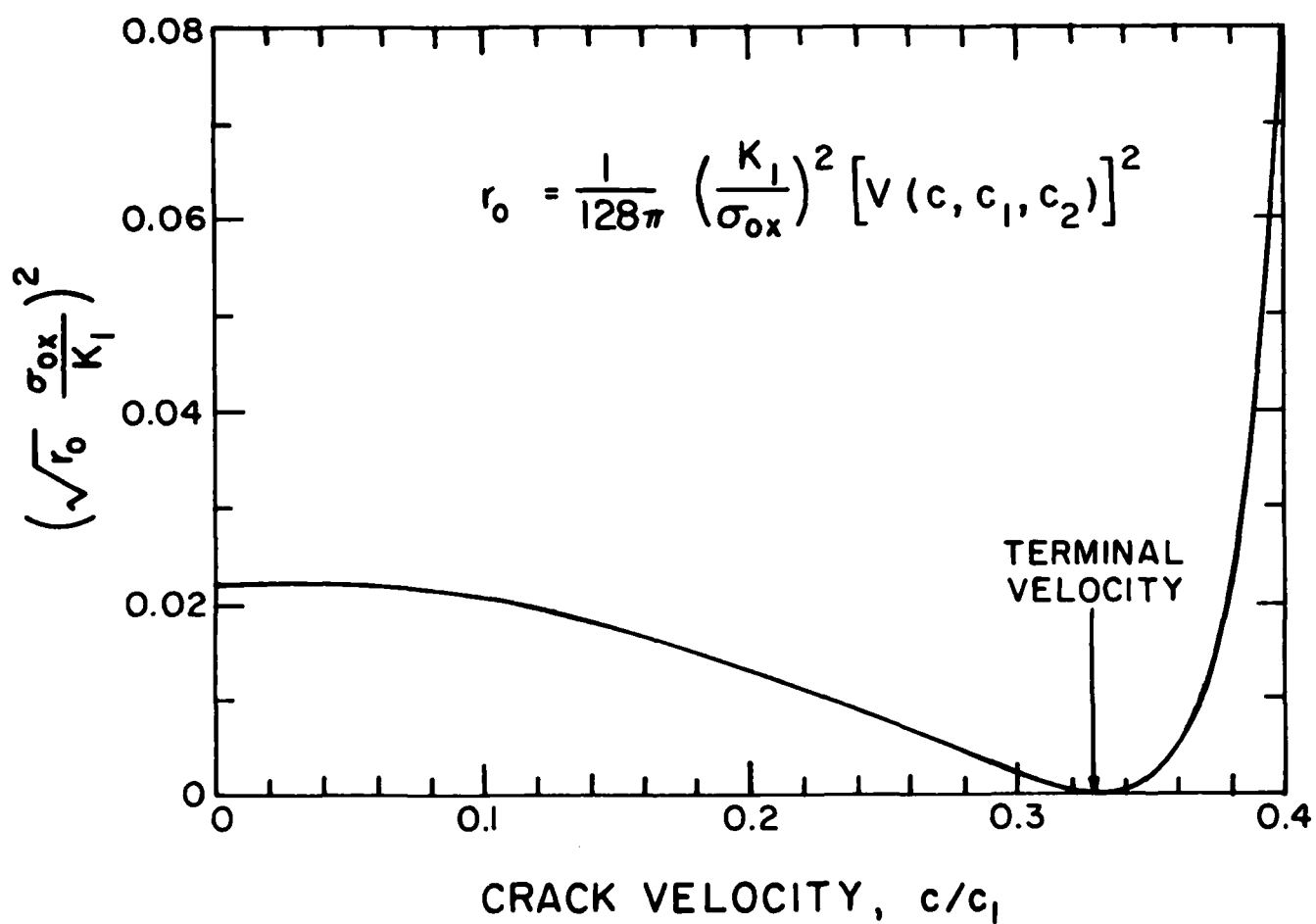
FIG. 1. NON DIMENSIONALIZED REMOTE STRESS vs CRACK VELOCITY.
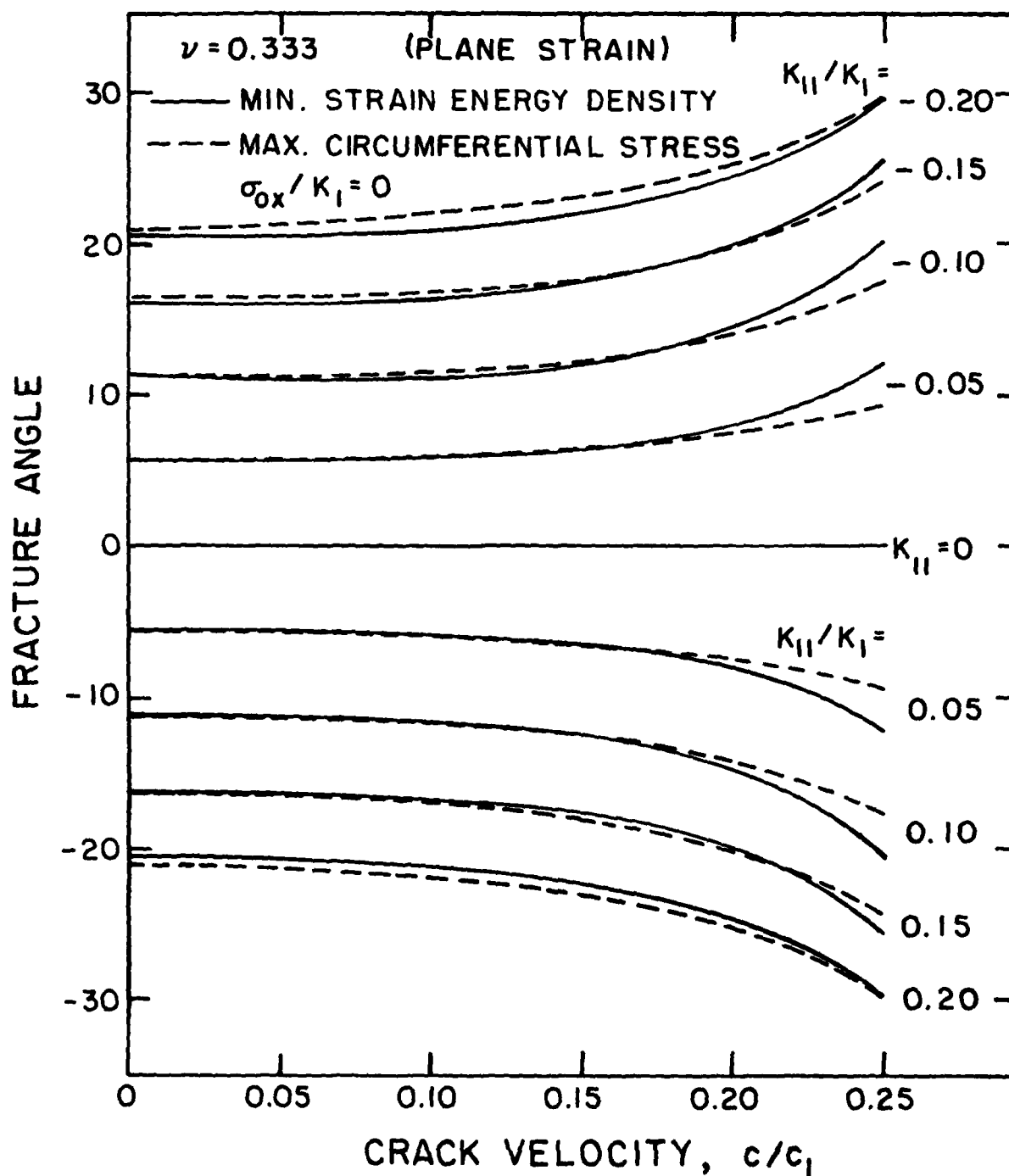
FIG. 2 . DYNAMIC CRACK EXTENSION ANGLE FOR MIXED MODE
LOADING BY MAX. CIRCUMFERENTIAL STRESS CRITERION
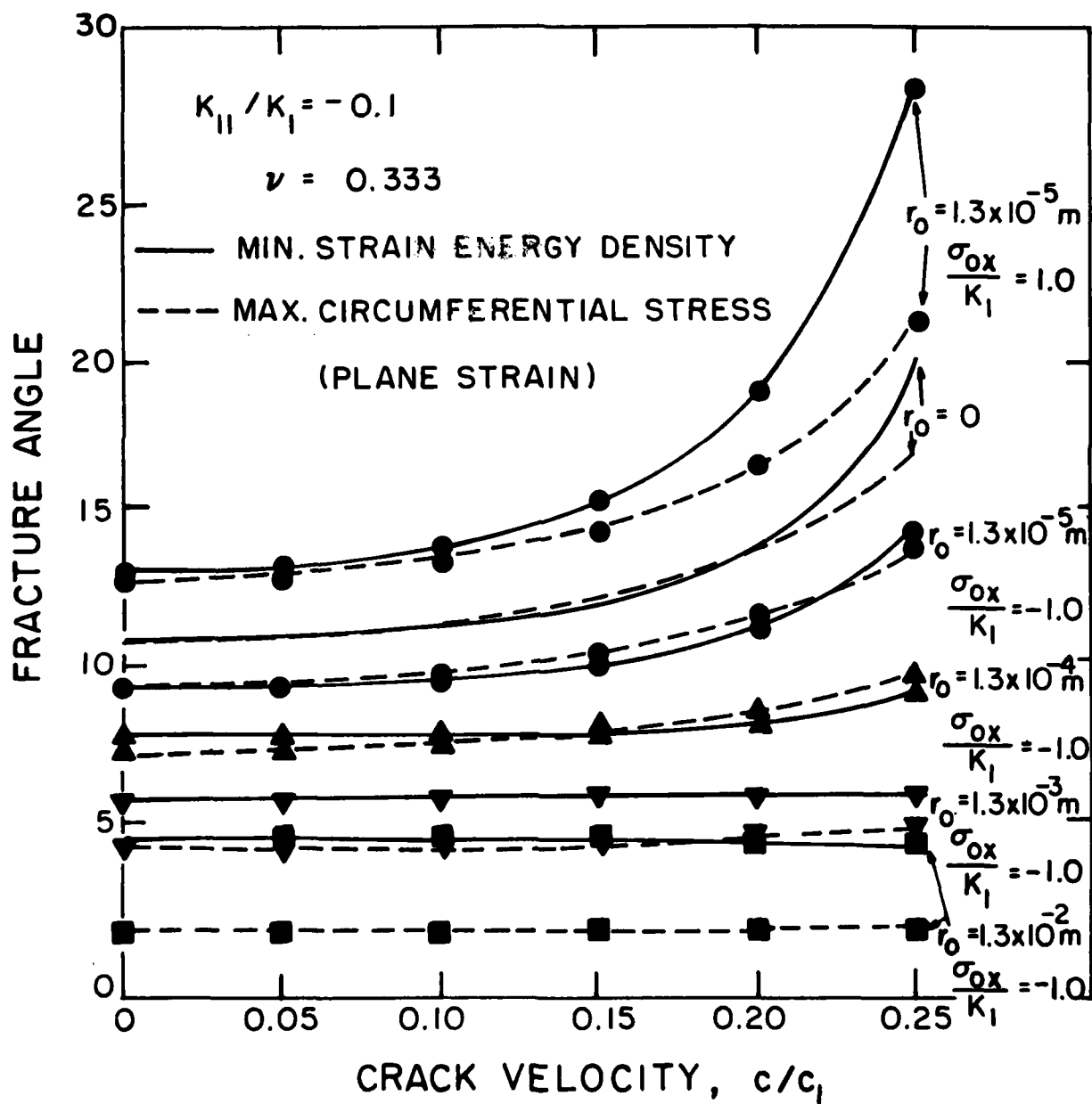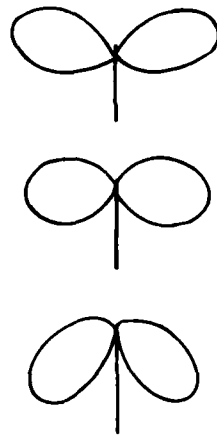AND MIN. STRAIN ENERGY DENSITY CRITERION WITHOUT
NON-SINGULAR STRESS.

FIG. 3. EFFECT OF REFERENCE RADIUS r_0 FOR PREDICTING DYNAMIC CRACK EXTENSION ANGLE AT $K_{II}/K_I = -0.1$ BY MAX. CIRCUMFERENTIAL STRESS CRITERION AND MINIMUM STRAIN ENERGY DENSITY CRITERION WITH VARYING NON–SINGULAR STRESS.

CRACK INSTABILITY BY DYNAMIC PHOTOELASTICITY
UNDER PURE MODE I CONDITIONS

$\sigma_{ox} > 0$ $\sigma_{ox} = 0$ $\sigma_{ox} < 0$

INSTABILITY   STABLE   LESS UNSTABLE

FRACTURE PATH PREDICTIONS BY DYNAMIC PHOTOELASTICITY
UNDER MIXED MODE CONDITIONS

$\theta_{02} > \theta_{01}$ $\theta_{01} = \theta_{02}$ $\theta_{02} > \theta_{01}$

$\theta = \theta_{01}$ $\theta_{O} = \theta_{02}$ $\theta = \theta_{01}$ $\theta = \theta_{02}$ $\theta = \theta_{01}$ $\theta_{O} = \theta_{02}$
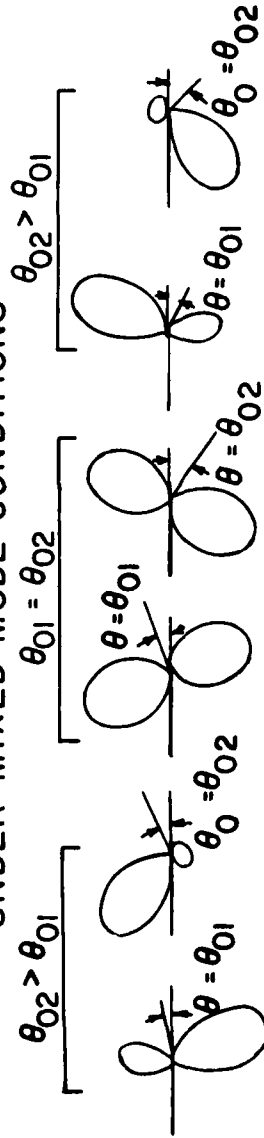
$K_{II}/K_I < 0$ $K_{II}/K_I < 0$ $K_{II}/K_I > 0$ $K_{II}/K_I > 0$
$\sigma_{ox} < 0$ $\sigma_{ox} > 0$ $\sigma_{ox} = 0$ $\sigma_{ox} = 0$ $\sigma_{ox} < 0$ $\sigma_{ox} > 0$

FIG. 4. EXPECTED FRACTURE PATHS BY DYNAMIC PHOTOELASTICITY.

(a) FIFTH FRAME 100 μ SECONDS

(b) EIGTH FRAME 130 μ SECONDS
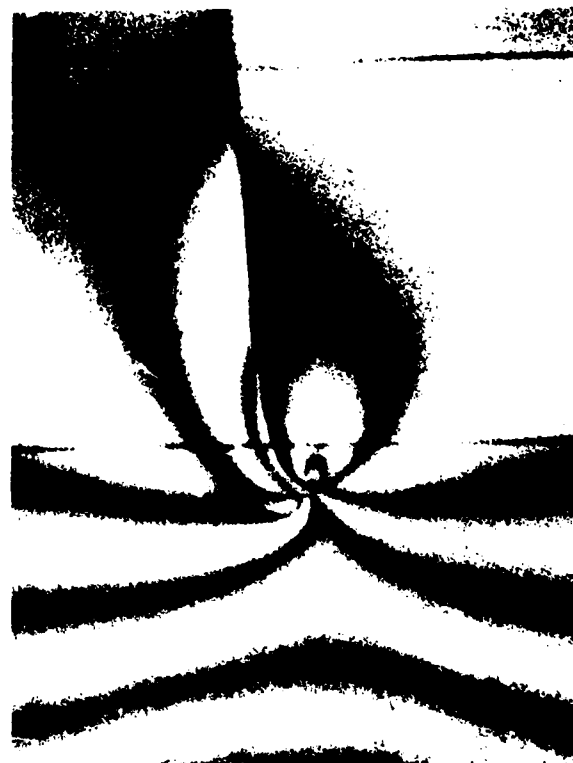
(c) TENTH FRAME 160 μ SECONDS

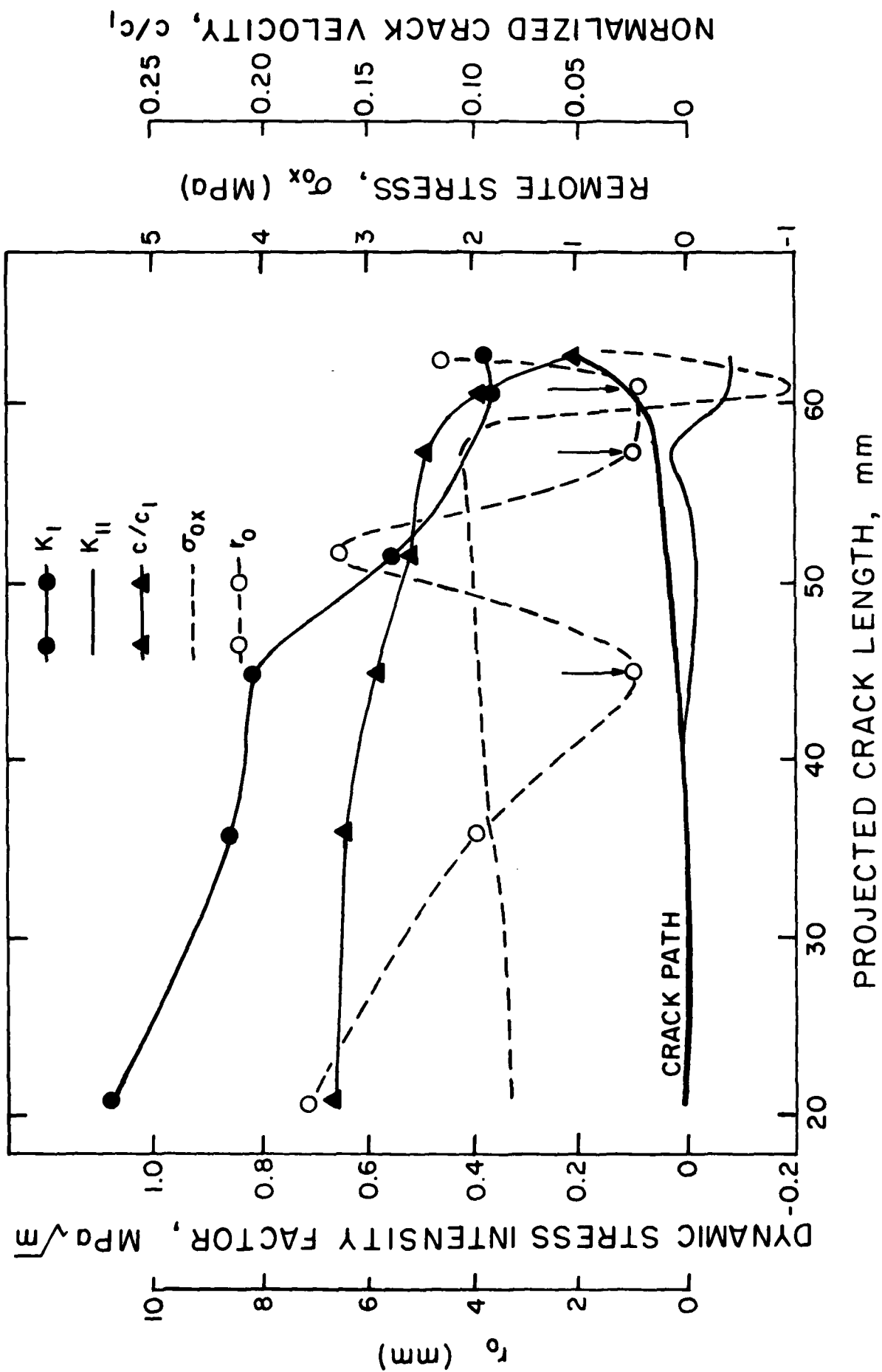FIG. 5 . TYPICAL DYNAMIC ISOCHROMATICS OF A CURVED CRACK HOMOLITE-100 NOTCH BEND SPECIMEN NO. 6- CO51074.

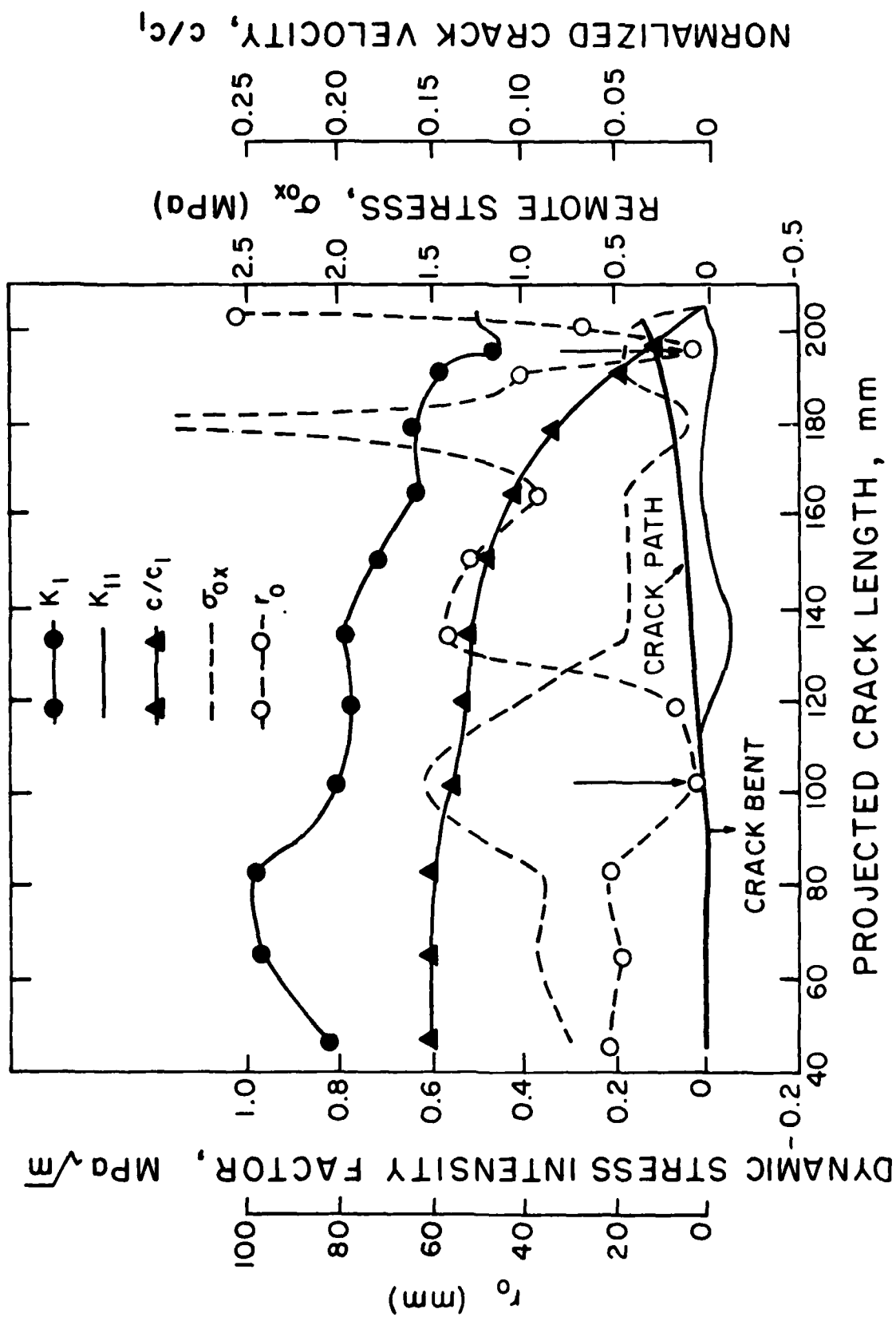FIG. 6. MODE I AND MODE II DYNAMIC STRESS INTENSITY FACTORS OF THE CURVED CRACK SHOWN IN FIG. 5.

FIG. 7. MODE I AND MODE II DYNAMIC STRESS INTENSITY FACTORS OF SLIGHTLY CURVED CRACK IN A SINGLE-EDGED-NOTCH (SEN) TENSION PLATE. HOMALITE-100, SPECIMEN NO. B12.
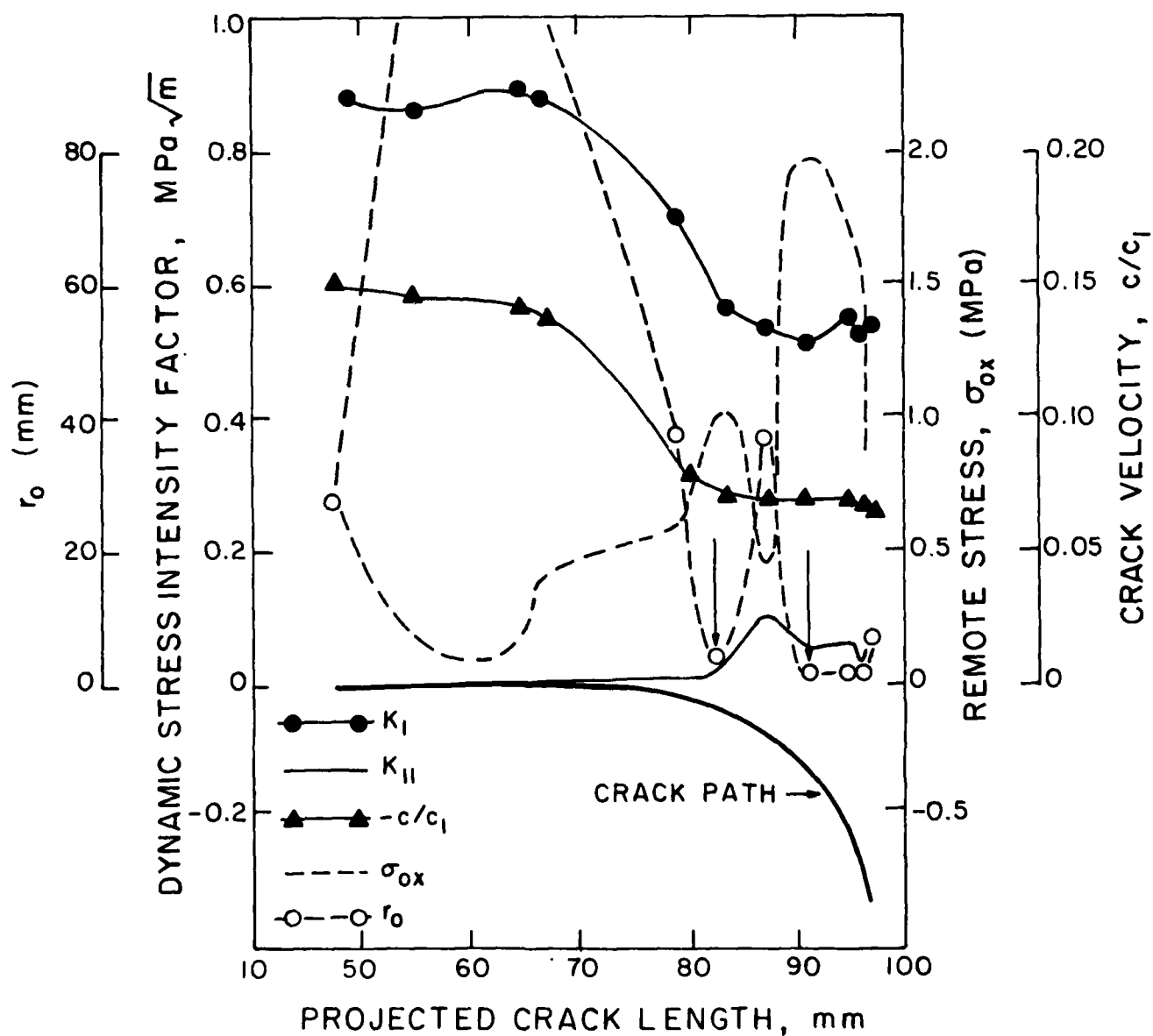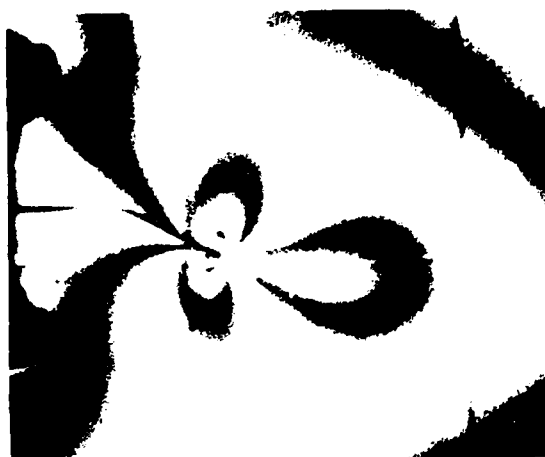
FIG. 8. MODE I AND MODE II DYNAMIC STRESS INTENSITY FACTORS OF A CURVED CRACK IN A WEDGE LOADED RECTANGULAR DOUBLE CANTILEVER SPECIMEN, HOMOLITE -100, SPECIMEN NO. L7B - 051573.
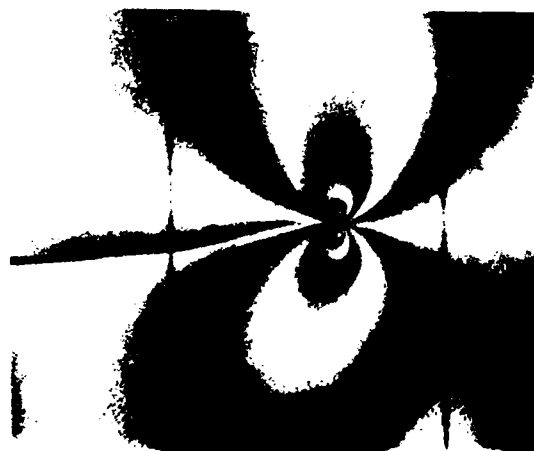
(a) SEVENTH FRAME 150 μSECONDS

(b) TENTH FRAME 255 μSECONDS

(c)TWELFTH FRAME 315 μSECONDS

(d) FOURTEENTH FRAME 370 μSECONDS

(e) FITEENTH FRAME 390 μSECONDS

FIG. 9 .TYPICAL DYNAMIC ISOCHROMATICS OF A CURVED CRACK. HOMALITE-100
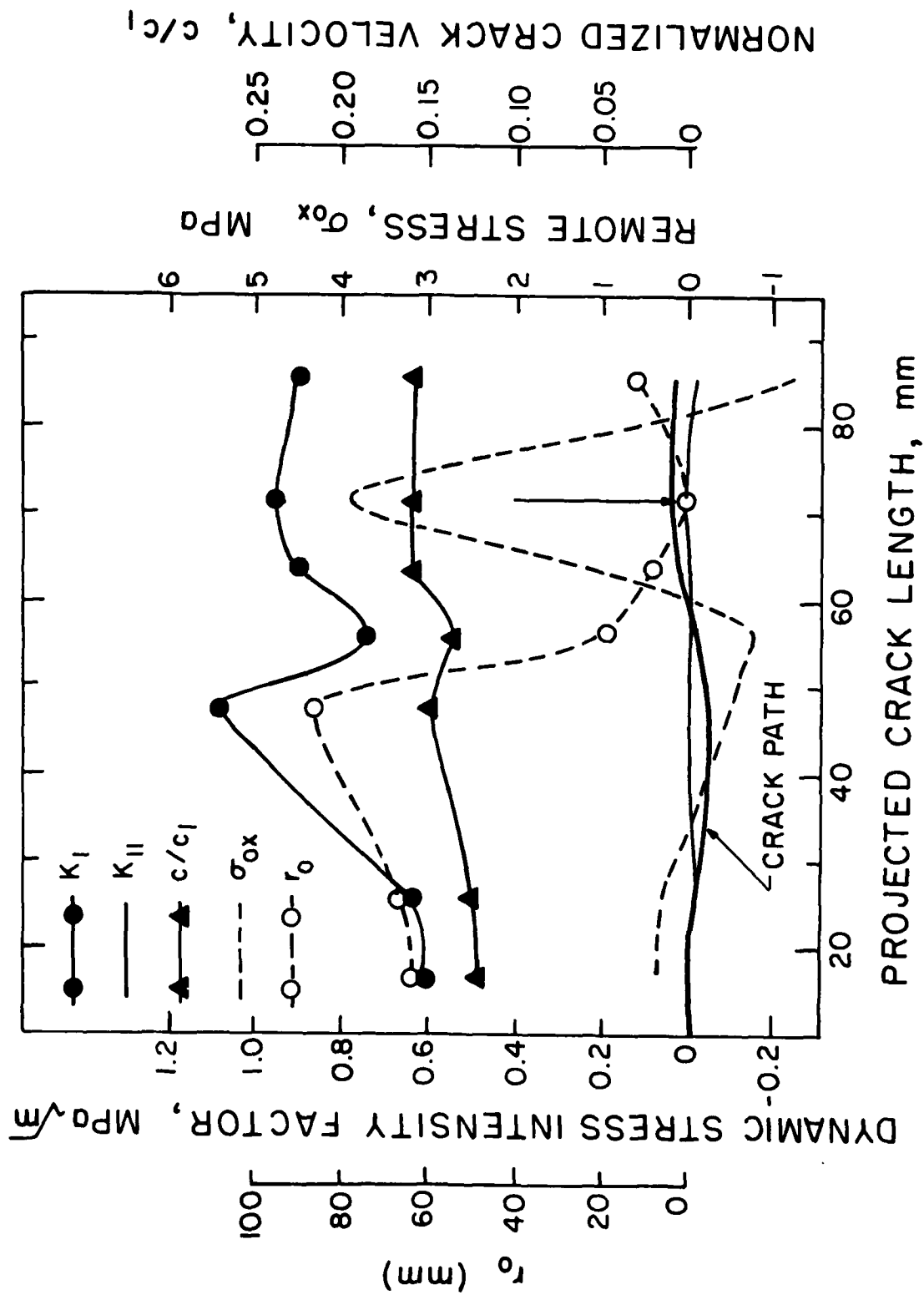EDGE- CRACKED TENSION PLATE IMPACTED BY A FLAT NOSE PROJECTILE,
SPECIMEN NO. 21-W090771.

FIG.10. MODE I AND II DYNAMIC STRESS INTENSITY FACTORS OF A CURVED CRACK IN A ANGLE - EDGED - NOTCH TENSION PLATE IMPACTED BY A FLAT NOSE PROJECTILE. HOMALITE -100 SPECIMEN NO. 21-W090771.

Part 1 - Government
Administrative and Liaison Activities

Office of Naval Research
Department of the Navy
Arlington, Virginia 22217
Attn: Code 474 (2)
Code 471
Code 200

Director
Office of Naval Research
Branch Office
666 Summer Street
Boston, Massachusetts 02210

Director
Office of Naval Research
Branch Office
536 South Clark Street
Chicago, Illinois 60605

Director
Office of Naval Research
New York Area Office
715 Broadway - 5th Floor
New York, New York 10003

Director
Office of Naval Research
Branch Office
1030 East Green Street
Pasadena, California 91106

Naval Research Laboratory (6)
Code 2627
Washington, D.C. 20375

Defense Documentation Center (12)
Cameron Station
Alexandria, Virginia 22314

Navy

Underaea Explosion Research Division
Naval Ship Research and Development
Center
Norfolk Naval Shipyard
Portsmouth, Virginia 23709
Attn: Dr. E. Palmer, Code 177

Navy (Con't.)

Naval Research Laboratory
Washington, D.C. 20375
Attn: Code 8400
8410
8430
8440
6300
6390
6380

David W. Taylor Naval Ship Research
and Development Center
Annapolis, Maryland 21402
Attn: Code 2740
28
281

Naval Weapons Center
China Lake, California 93555
Attn: Code 4062
4520

Commanding Officer
Naval Civil Engineering Laboratory
Code L31
Port Hueneme, California 93041

Naval Surface Weapons Center
White Oak
Silver Spring, Maryland 20910
Attn: Code R-10
G-402
K-82

Technical Director
Naval Ocean Systems Center
San Diego, California 92152

Supervisor of Shipbuilding
U.S. Navy
Newport News, Virginia 23607

Navy Underwater Sound
Reference Division
Naval Research Laboratory
P.O. Box 8337
Orlando, Florida 32806

Navy (Con't.)

Chief of Naval Operations
Department of the Navy
Washington, D.C. 20350
Attn: Code OP-098

Strategic Systems Project Office
Department of the Navy
Washington, D.C. 20376
Attn: NSP-200

Naval Air Systems Command
Department of the Navy
Washington, D.C. 20361
Attn: Code 5302 (Aerospace and Structures)
604 (Technical Library)
320B (Structures)

Naval Air Development Center
Warminster, Pennsylvania 18974
Attn: Aerospace Mechanics
Code 606

U.S. Naval Academy
Engineering Department
Annapolis, Maryland 21402

Naval Facilities Engineering Command
200 Stovall Street
Alexandria, Virginia 22332
Attn: Code 03 (Research and Development)
04B
045
14114 (Technical Library)

Naval Sea Systems Command
Department of the Navy
Washington, D.C. 20362
Attn: Code 05H
312
322
323
05R
32R

Navy (Con't.)

Commander and Director
David W. Taylor Naval Ship
Research and Development Center
Bethesda, Maryland 20084
Attn: Code 042
17
172
173
174
1800
1844
012.2
1900
1901
1945
1960
1962

Naval Underwater Systems Center
Newport, Rhode Island 02840
Attn: Dr. R. Trainor

Naval Surface Weapons Center
Dahlgren Laboratory
Dahlgren, Virginia 22448
Attn: Code G04
G20

Technical Director
Mare Island Naval Shipyard
Vallejo, California 94592

U.S. Naval Postgraduate School
Library
Code 0384
Monterey, California 93940

Webb Institute of Naval Architecture
Attn: Librarian
Crescent Beach Road, Glen Cove
Long Island, New York 11542

Army

Commanding Officer (2)
U.S. Army Research Office
P.O. Box 12211
Research Triangle Park, NC 27709
Attn: Mr. J. J. Murray, CRD-AA-IP

Army (Con't.)

Watervliet Arsenal
MAGGS Research Center
Watervliet, New York 12189
Attn: Director of Research

U.S. Army Materials and Mechanics
Research Center
Watertown, Massachusetts 02172
Attn: Dr. R. Shea, DRXMR-T

U.S. Army Missile Research and
Development Center
Redstone Scientific Information
Center
Chief, Document Section
Redstone Arsenal, Alabama 35809

Army Research and Development
Center
Fort Belvoir, Virginia 22060

NASA

National Aeronautics and Space
Administration
Structures Research Division
Langley Research Center
Langley Station
Hampton, Virginia 23365

National Aeronautics and Space
Administration
Associate Administrator for Advanced
Research and Technology
Washington, D.C. 20546

Air Force

Wright-Patterson Air Force Base
Dayton, Ohio 45433
Attn: AFFDL (FB)
(FBR)
(FBE)
(FBS)
AFML (MBM)

Air Force (Con't.)

Chief Applied Mechanics Group
U.S. Air Force Institute of Technology
Wright-Patterson Air Force Base
Dayton, Ohio 45433

Chief, Civil Engineering Branch
WLRC, Research Division
Air Force Weapons Laboratory
Kirtland Air Force Base
Albuquerque, New Mexico 87117

Air Force Office of Scientific Research
Bolling Air Force Base
Washington, D.C. 20305
Attn: Mechanics Division

Department of the Air Force
Air University Library
Maxwell Air Force Base
Montgomery, Alabama 36112

Other Government Activities

Commandant
Chief, Testing and Development Division
U.S. Coast Guard
1300 E Street, NW.
Washington, D.C. 20226

Technical Director
Marine Corps Development
and Education Command
Quantico, Virginia 22134

Director Defense Research
and Engineering
Technical Library
Room 3C128
The Pentagon
Washington, D.C. 20301

Other Government Activities (Con't)

Dr. M. Gaus
National Science Foundation
Environmental Research Division
Washington, D.C. 20550

Library of Congress
Science and Technology Division
Washington, D.C. 20540

Director
Defense Nuclear Agency
Washington, D.C. 20305
Attn: SPSS

Mr. Jerome Persh
Staff Specialist for Materials
and Structures
OUDRAE, The Pentagon
Room 3D1089
Washington, D.C. 20301

Chief, Airframe and Equipment Branch
FS-120
Office of Flight Standards
Federal Aviation Agency
Washington, D.C. 20553

National Academy of Sciences
National Research Council
Ship Hull Research Committee
2101 Constitution Avenue
Washington, D.C. 20418
Attn: Mr. A. R. Lytle

National Science Foundation
Engineering Mechanics Section
Division of Engineering
Washington, D.C. 20550

Picatinny Arsenal
Plastics Technical Evaluation Center
Attn: Technical Information Section
Dover, New Jersey 07801

Maritime Administration
Office of Maritime Technology
14th and Constitution Avenue, NW.
Washington, D.C. 20230

PART 2 - Contractors and Other Technical
Collaborators

Universities

Dr. J. Tinsley Oden
University of Texas at Austin
345 Engineering Science Building
Austin, Texas 78712

Professor Julius Miklowitz
California Institute of Technology
Division of Engineering
and Applied Sciences
Pasadena, California 91109

Dr. Harold Liebowitz, Dean
School of Engineering and
Applied Science
George Washington University
Washington, D.C. 20052

Professor Eli Sternberg
California Institute of Technology
Division of Engineering and
Applied Sciences
Pasadena, California 91109

Professor Paul M. Naghdi
University of California
Department of Mechanical Engineering
Berkeley, California 94720

Professor A. J. Durelli
Oakland University
School of Engineering
Rochester, Missouri 48063

Professor F. L. DiMaggio
Columbia University
Department of Civil Engineering
New York, New York 10027

Professor Norman Jones
The University of Liverpool
Department of Mechanical Engineering
P. O. Box 147
Brownlow Hill
Liverpool L69 3BX
England

Professor E. J. Skudrzyk
Pennsylvania State University
Applied Research Laboratory
Department of Physics
State College, Pennsylvania 16801

Universities (Con't.)

Professor J. Kloosner
Polytechnic Institute of New York
Department of Mechanical and
  Aerospace Engineering
333 Jay Street
Brooklyn, New York 11201

Professor R. A. Schapery
Texas A&M University
Department of Civil Engineering
College Station, Texas 77843

Professor Walter D. Pilkey
University of Virginia
Research Laboratories for the
  Engineering Sciences and
  Applied Sciences
Charlottesville, Virginia 22901

Professor K. D. Willmert
Clarkson College of Technology
Department of Mechanical Engineering
Potsdam, New York 13676

Dr. Walter E. Haisler
Texas A&M University
Aerospace Engineering Department
College Station, Texas 7/843

Dr. Hussein A. Kamel
University of Arizona
Department of Aerospace and
  Mechanical Engineering
Tucson, Arizona 85721

Dr. S. J. Fenves
Carnegie-Mellon University
Department of Civil Engineering
Schenley Park
Pittsburgh, Pennsylvania 15213

Dr. Ronald L. Huston
Department of Engineering Analysis
University of Cincinnati
Cincinnati, Ohio 45221

Professor G. C. M. Sih
Lehigh University
Institute of Fracture and
  Solid Mechanics
Bethlehem, Pennsylvania 18015

Professor Albert S. Kobayashi
University of Washington
Department of Mechanical Engineering
Seattle, Washington 98105

Professor Daniel Frederick
Virginia Polytechnic Institute and
  State University
Department of Engineering Mechanics
Blacksburg, Virginia 24061

Professor A. C. Eringen
Princeton University
Department of Aerospace and
  Mechanical Sciences
Princeton, New Jersey 08540

Professor E. H. Lee
Stanford University
Division of Engineering Mechanics
Stanford, California 94305

Professor Albert I. King
Wayne State University
Biomechanics Research Center
Detroit, Michigan 48202

Dr. V. R. Hodgson
Wayne State University
School of Medicine
Detroit, Michigan 48202

Dean B. A. Boley
Northwestern University
Department of Civil Engineering
Evanston, Illinois 60201

Professor P. G. Hodge, Jr.
University of Minnesota
Department of Aerospace Engineering
  and Mechanics
Minneapolis, Minnesota 55455

Dr. D. C. Drucker
University of Illinois
Dean of Engineering
Urbana, Illinois 61801

Professor N. M. Newmark
University of Illinois
Department of Civil Engineering
Urbana, Illinois 61803

Professor E. Reissner
University of California, San Diego
Department of Applied Mechanics
La Jolla, California 92037

Professor William A. Nash
University of Massachusetts
Department of Mechanics and
  Aerospace Engineering
Amherst, Massachusetts 01002

Professor G. Herrmann
Stanford University
Department of Applied Mechanics
Stanford, California 94305

Professor J. D. Achenbach
Northwest University
Department of Civil Engineering
Evanston, Illinois 60201

Professor S. B. Dong
University of California
Department of Mechanics
Los Angeles, California 90024

Professor Burt Paul
University of Pennsylvania
Towne School of Civil and
  Mechanical Engineering
Philadelphia, Pennsylvania 19104

Professor H. W. Liu
Syracuse University
Department of Chemical Engineering
  and Metallurgy
Syracuse, New York 13210

Professor S. Bodner
Technion R&D Foundation
Haifa, Israel

Professor Werner Goldsmith
University of California
Department of Mechanical Engineering
Berkeley, California 94720

Professor R. S. Rivlin
Lehigh University
Center for the Application
  of Mathematics
Bethlehem, Pennsylvania 18015

Professor F. A. Cozzarelli
State University of New York at
  Buffalo
Division of Interdisciplinary Studies
Karr Parker Engineering Building
Chemistry Road
Buffalo, New York 14214

Professor Joseph L. Rose
Drexel University
Department of Mechanical Engineering
  and Mechanics
Philadelphia, Pennsylvania 19104

Professor B. K. Donaldson
University of Maryland
Aerospace Engineering Department
College Park, Maryland 20742

Professor Joseph A. Clark
Catholic University of America
Department of Mechanical Engineering
Washington, D.C. 20064

Universities (Con't)

Dr. Samuel B. Batdorf
University of California
School of Engineering
  and Applied Science
Los Angeles, California 90024

Professor Isaac Fried
Boston University
Department of Mathematics
Boston, Massachusetts 02215

Professor E. Krempl
Rensselaer Polytechnic Institute
Division of Engineering
Engineering Mechanics
Troy, New York 12181

Dr. Jack R. Vinson
University of Delaware
Department of Mechanical and Aerospace
  Engineering and the Center for
  Composite Materials
Newark, Delaware 19711

Dr. J. Duffy
Brown University
Division of Engineering
Providence, Rhode Island 02912

Dr. J. L. Swedlow
Carnegie-Mellon University
Department of Mechanical Engineering
Pittsburgh, Pennsylvania 15213

Dr. V. K. Varadan
Ohio State University Research Foundation
Department of Engineering Mechanics
Columbus, Ohio 43210

Dr. Z. Hashin
University of Pennsylvania
Department of Metallurgy and
  Materials Science
College of Engineering and
  Applied Science
Philadelphia, Pennsylvania 19104

Dr. Jackson C. S. Yang
University of Maryland
Department of Mechanical Engineering
College Park, Maryland 20742

Professor T. Y. Chang
University of Akron
Department of Civil Engineering
Akron, Ohio 44325

Professor Charles W. Bert
University of Oklahoma
School of Aerospace, Mechanical,
  and Nuclear Engineering
Norman, Oklahoma 73019

Professor Satya N. Atluri
Georgia Institute of Technology
School of Engineering and
  Mechanics
Atlanta, Georgia 30332

Professor Graham F. Carey
University of Texas at Austin
Department of Aerospace Engineering
  and Engineering Mechanics
Austin, Texas 78712

Dr. S. S. Wang
University of Illinois
Department of Theoretical and
  Applied Mechanics
Urbana, Illinois 61801

Industry and Research Institutes

Dr. Norman Hobbs
Kaman AviDyne
Division of Kaman
  Sciences Corporation
Burlington, Massachusetts 01803

Argonne National Laboratory
Library Services Department
9700 South Cass Avenue
Argonne, Illinois 60440

Industry and Research Institutes (Con't)

Dr. M. C. Junger
Cambridge Acoustical Associates
54 Rindge Avenue Extension
Cambridge, Massachusetts 02140

Dr. V. Godino
General Dynamics Corporation
Electric Boat Division
Groton, Connecticut 06340

Dr. J. E. Greenspon
J. C. Engineering Research Associates
3831 Menlo Drive
Baltimore, Maryland 21215

Newport News Shipbuilding and
  Dry Dock Company
Library
Newport News, Virginia 23607

Dr. W. F. Bozich
McDonnell Douglas Corporation
5301 Bolsa Avenue
Huntington Beach, California 92647

Dr. H. N. Abramson
Southwest Research Institute
8500 Culebra Road
San Antonio, Texas 78284

Dr. R. C. DeHart
Southwest Research Institute
8500 Culebra Road
San Antonio, Texas 78284

Dr. M. L. Baron
Weidlinger Associates
110 East 59th Street
New York, New York 10022

Dr. T. L. Geers
Lockheed Missiles and Space Company
3251 Hanover Street
Palo Alto, California 94304

Mr. William Caywood
Applied Physics Laboratory
Johns Hopkins Road
Laurel, Maryland 20810

Industry and Research Institutes (Con't)

Dr. Robert E. Dunham
Pacifica Technology
P.O. Box 148
Del Mar, California 92014

Dr. M. F. Kanninen
Battelle Columbus Laboratories
505 King Avenue
Columbus, Ohio 43201

Dr. A. A. Hochrein
Daedalean Associates, Inc
Springlake Research Road
15110 Frederick Road
Woodbine, Maryland 21797

Dr. James W. Jones
Swanson Service Corporation
P.O. Box 5415
Huntington Beach, California 92646

Dr. Robert E. Nickell
Applied Science and Technology
3344 North Torrey Pines Court
Suite 220
La Jolla, California 92037

Dr. Kevin Thomas
Westinghouse Electric Corp.
Advanced Reactors Division
P.O. Box 158
Madison, Pennsylvania 15663

REPORT DOCUMENTATION PAGE		READ INSTRUCTIONS BEFORE COMPLETING FORM
1. REPORT NUMBER TR 41	2. GOVT ACCESSION NO. AD-A107 238	3. RECIPIENT'S CATALOG NUMBER
4. TITLE (and Subtitle) DYNAMIC CRACK CURVING - A PHOTOELASTIC EVALUATION		5. TYPE OF REPORT & PERIOD COVERED Technical Report
		6. PERFORMING ORG. REPORT NUMBER TR-41
7. AUTHOR(s) M. Ramulu and A. S. Kobayashi		8. CONTRACT OR GRANT NUMBER(s) N00014-76-C-0060
9. PERFORMING ORGANIZATION NAME AND ADDRESS Dept. of Mechanical Engineering 6U-10 University of Washington Seattle, WA 98195		10. PROGRAM ELEMENT, PROJECT, TASK AREA & WORK UNIT NUMBERS NR 064-478
11. CONTROLLING OFFICE NAME AND ADDRESS Office of Naval Research Arlington, VA 22217		12. REPORT DATE October 1981
		13. NUMBER OF PAGES 26
14. MONITORING AGENCY NAME & ADDRESS(If different from Controlling Office)		15. SECURITY CLASS. (of this report) Unclassified
		15a. DECLASSIFICATION/DOWNGRADING SCHEDULE

16. DISTRIBUTION STATEMENT (of this Report)

Unlimited

DISTRIBUTION STATEMENT A
Approved for public release;
Distribution Unlimited

17. DISTRIBUTION STATEMENT (of the abstract entered In Block 20, If different from Report)

18. SUPPLEMENTARY NOTES

19. KEY WORDS (Continue on reverse side If necessary and Identify by block number)

Dynamic stress intensity factors, dynamic fracture mechanics, dynamic crack curving, dynamic photoelasticity, maximum circumferential stress, minimum strain energy density.

20. ABSTRACT (Continue on reverse side If necessary and Identify by block number)

A dynamic crack curving criterion, which is valid under combined modes I and II or mode I loading and which is based on either the maximum circumferential stress or minimum strain energy density factor at a reference distance of
$$r_0 = \frac{1}{128\pi}\left[\frac{K_I}{\sigma_{ox}} \cdot V\ (c,c_1,c_2)\right]^2$$
crack deformation, is developed. Directional

stability of a mode I crack propagation is attained when $r_o > r_c$, where r_c for

Homalite-100 was determined from dynamic photoelastic experiments.